Multifunctional chitosan–magnetic graphene quantum dot nanocomposites for the release of therapeutics from detachable and non-detachable biodegradable microneedle arrays

Justin, R., & Chen, B. (2018). Multifunctional chitosan–magnetic graphene quantum dot nanocomposites for the release of therapeutics from detachable and non-detachable biodegradable microneedle arrays. *Interface Focus*, *8*(3), [20170055]. https://doi.org/10.1098/rsfs.2017.0055

Published in:
Interface Focus

Document Version:
Peer reviewed version

Queen's University Belfast - Research Portal:
Link to publication record in Queen's University Belfast Research Portal

Multifunctional chitosan–magnetic graphene quantum dot nanocomposites for the release of therapeutics from detachable and non-detachable biodegradable microneedle arrays

Richard Justin[1] and Biqiong Chen[2]*

[1]Department of Materials Science and Engineering, University of Sheffield, Mappin Street, Sheffield S1 3JD, United Kingdom.

[2]School of Mechanical and Aerospace Engineering, Queen's University Belfast, Stranmillis Road, Belfast BT9 5AH, United Kingdom.

***Author for Correspondence:**

Biqiong Chen

e-mail: b.chen@qub.ac.uk

Abstract

Biodegradable chitosan–magnetic graphene quantum dot (MGQD) nanocomposites were prepared and investigated for the release of small and large molecular weight (MWt) therapeutics from detachable and non-detachable biodegradable microneedle arrays. The presence of MGQDs in chitosan increased the electrical conductivity and biodegradation rate of chitosan whilst maintaining its mechanical properties. The detachable microneedle arrays were created by including a water-soluble ring of poly(ethylene glycol) (PEG) at the base of the microneedle, which enabled the rapid detachment of the microneedle shaft from the base. The PEG ring did not impede the microneedle array performance, with mechanical properties and a drug release profile of low MWt lidocaine hydrochloride similar to microneedle arrays without the ring. Without the PEG ring, the chitosan–MGQD microneedles were electrically conductive and allowed for electrically stimulated release of large MWt therapeutics which was challenging without the stimulation. These results demonstrate that chitosan nanocomposites containing MGQDs with intrinsic photoluminescent and supermaganetic properties are promising materials for developing multifunctional microneedles for targeted and tracked transdermal drug delivery.

Keywords: Graphene, biopolymer, nanocomposite, microneedle, drug delivery.

Introduction

Chemically oxidised graphene, known as graphene oxide (GO) [1] has been researched as a drug carrier that may work more efficiently than free therapeutics [2,3], as a biosensor to detect a wide range of items such as the rotavirus [4], and glucose [5], as a photothermal ablation agent against cancer tumours [6], and as fluorescent imaging agents [7]. Graphene–based nanoparticles have been integrated into polymers to form nanocomposites that can be used for drug delivery, such as the electrically stimulated release of dexamethasone [8] and the pH-sensitive release from a hydrogel of GO and gelatin [9]. Chitosan was used as the polymer matrix for nanocomposites containing GO [10] and reduced graphene oxide (rGO) [11] for transdermal drug delivery. These nanocomposites possessed better mechanical properties and improved drug release profiles over pristine chitosan, as well as novel functionality such as pH-sensitive release, and electrical conductivity [10,11].

Other nanoparticles that are of interest to nanomedicine include magnetic quantum dots (MQDs) that can be synthesised by doping quantum dots (QDs) of cadmium–selenium (Cd–Se) or cadmium–telluride (Cd–Te) with manganese [12] or cobalt [13], or by encapsulating magnetite or CdSe in silica spheres [14]. The delivery of the drug could be site specific as the MQDs could be manipulated by magnetic fields. Recently, QDs made from rGO chemically coated with iron oxide (from herein known as magnetic graphene quantum dots, MGQDs) were reported by our group [3], and were shown to be of low toxicity at low concentrations, photoluminescent, and superparamagnetic to form a system which allows for both targeted and tracked drug delivery. Chitosan–GQD nanocomposite microneedles were also prepared by our group that allowed for the passive release of lidocaine hydrochloride (LH) and the electrically stimulated release of bovine serum albumin (BSA) [15]. These nanocomposites possessed higher electrical conductivity than pristine chitosan and allowed for photoluminescent tracking/imaging of the therapeutic [15].

Strong, biodegradable polymer nanocomposites could find use in microneedle arrays for transdermal drug delivery. Chitosan was selected as the biodegradable polymer matrix to manufacture nanocomposite microneedles because it is biocompatible, renewable (sourced from chitin extracted from the shells of sea crustaceans), and easy to process [16]. Typically, microneedle arrays are solid, conical microstructures with dimensions less than one millimetre. Microneedle arrays use the conical projections to pierce through the stratum corneum (SC) and to expose the viable epidermis, a region with numerous blood vessels but no nerves [17]. Microneedles have a high level of patient compliance with minimal irritation to the skin or pain to the patient [18], and offer enhanced immune response to vaccinations than conventional hypodermic injection [19] and the ability to deliver a wide range of therapeutics, for example desmopressin [20] and insulin [21].

The release of the encapsulated therapeutic from polymer microneedle arrays typically is dependent upon the biodegradation (for example, polylactide) or the dissolution rate of the polymer within bodily fluids. If these rates are too slow, it will need long treatment times to give the required dosage, in which case the prolonged placement of the microneedle patch on the skin may cause irritation and/or impede the healing process of the SC [22]. To counter this problem, microneedle arrays have been developed with detachable microneedles that will stay in the body after the backing patch has been removed, such as arrowhead–shaped microneedles tips that detach from the main microneedle shaft when it is removed from the body [23]. But these approaches limit the size of the therapeutic dosage delivered as the drug is limited to just the arrowhead tip and not the shaft, and may also incur extra costs for manufacturing and assembling the arrowheads.

The aim of this work is to develop a novel multifunctional microneedle system with a simple detachable design for future targeted and tracked transdermal drug delivery, based on biodegradable chitosan and photoluminescent and superparamagnetic iron oxide–graphene

quantum dot nanocomposites. The new design of the microneedle array allows for the quick separation of the microneedle shafts from the base, while maintaining the capability of the main shaft to encapsulate a large amount of therapeutic. MGQDs were synthesised and characterised in our previous work [3], utilising hydrothermal reduction of GO–IO to form sub 50 nm magnetic QDs. The MGQDs were combined with chitosan to form nanocomposites of various concentrations which were structurally characterised, and analysed for electrical, mechanical and biodegradation behaviour. The optimal nanocomposite was then chosen as the material to create multifunctional microneedle arrays, which were tested for mechanical integrity under standard skin-insertion loading conditions, as well as delivery of small and large molecular weight (MWt) therapeutics with and without application of an electrical stimulus. The creation of a detachable microneedle system was achieved through the introduction of a disc section at the base of the microneedle shaft that was made from a water soluble biopolymer poly(ethylene glycol) (PEG); the PEG can be rapidly dissolved by the body fluid which allows for the microneedles to detach from the base patch enabling the removal of the patch soon after its application. The effect of this new additional ring on the mechanical and drug release behaviour of the original microneedle array was assessed.

Experimental

Materials

The following chemicals were reagent grade and used as purchased from Sigma Aldrich; acetic acid (>99.7%), sulphuric acid (95–98%), hydrogen peroxide (29–32% in H_2O), potassium permanganate (97%), sodium nitrate (>99%), lidocaine hydrochloride (LH, >99%), ferrous chloride tetrahydrate ($FeCl_2$–$4H_2O$, >99%), ferric chloride hexahydrate ($FeCl_3$–$6H_2O$, 97%), fluorescein sodium (FL), lysozyme (from chicken egg white, ~100,000

U mg^{-1}), fluorescein sodium labelled–bovine serum albumin (BSA), PEGs (MWt's = 10k, 20k and 35k Da) and graphite powder (≤20 μm). Chitosan (MWt = 100k–300k Da, Acros Scientific) and phosphate buffered saline (PBS) tablets (pH = 7.4) were purchased from Fisher Scientific.

Preparation of MGQDs

The method to prepare MGQDs has been described in our previous work [3]. Briefly, GO was synthesised from graphite using a modified Hummers method [1], purified and exfoliated in distilled water, and lyophilised in a freeze drier (Labconco FreeZone Triad). $FeCl_2$–$4H_2O$ (5.4 g) and $FeCl_3$–$6H_2O$ (4 g) were dissolved in 135 ml distilled water. GO (1 g) was sonicated in 150 ml distilled water for 1 h, and ammonium hydroxide was used to raise the pH to 8. The iron salt solution and the GO suspension were added together and the pH was raised to 10 by ammonium hydroxide. Under a nitrogen atmosphere, the mixture was stirred for 2 h, and the resultant precipitate, GO–IO, was washed with distilled water and ethanol. GO–IO was dispersed in distilled water (~3 mg ml^{-1}), and the suspension was hydrothermally reduced in a Parr Series 4000 autoclave (200 ºC for 10 h at 1.6 MPa). A dialysis bag (Fisher Scientific Biodesign Dialysis tubing, MWt cut off = 3.5k) was used to separate the quantum dots from larger particles. MGQDs were collected from the surrounding suspension and lyophilised for further use.

Drug loading onto MGQDs

Equal quantities of MGQD and either LH or BSA were added to distilled water to form an aqueous suspension of 0.1 mg ml^{-1} and stirred for 48 h. To remove the unbound therapeutic, the suspension was centrifuged (8000 rpm for 1 h) and dispersed in fresh distilled water several times. The resultant powder was lyophilised for use.

Preparation of chitosan–MGQD nanocomposites

The required amount (to form 0.25–5 wt.% nanocomposites) of the QDs (MGQD, MGQD–LH or MGQD–BSA) was dispersed with stirring and sonication in distilled water. Simultaneously, chitosan was added to 2 wt.% acetic acid in distilled water to form a 2 wt.% solution. When the chitosan was fully dissolved (typically left overnight at room temperature under stirring), the MGQD suspension was added under intense stirring and left stirring uncovered to allow the suspension to increase in viscosity (chitosan concentration of ~80 mg ml^{-1}). The mixture was degassed in a vacuum oven for 1 h at room temperature and poured into a mould to air dry.

Characterisation of nanocomposites

Fourier transform infra-red (FT-IR) spectroscopy was achieved with a resolution of 1 cm^{-1} between 400–4000 cm^{-1} on a Perkin Elmer Spectrum 100 with a diamond attenuated total reflectance (ATR) unit. X-ray diffraction (XRD) analysis on a Stoe Stadi P with Cu K_{α} irradiation (0.154 nm wavelength) was performed at 40 kV and 35 mA with a scanning speed of 1 ^{o} min^{-1}.

A Hounsfield twin column universal testing machine was used to mechanically test the nanocomposites with a 1 kN load cell and a 1 mm min^{-1} strain rate in accordance with ISO–527. Test specimens (number of specimens per material (n) $\geq$ 4) were punched from nanocomposite film and were dog-bone shaped (22 mm long, 2.7 mm wide, and 1 mm thick). Electrical conductivity (DC) was measured with an Agilent Technologies 34401A digital multimeter (n $\geq$ 3) with electrode contact points painted using silver paint (RS 186–3600) and applied voltage of 100 mV. Mass loss due to enzymatic biodegradation over 8 weeks of nanocomposite specimens (n = 5) in 37 ^{o}C PBS solution (pH = 7.4) with a 1.5 µg ml^{-1} concentration of lysozyme [24], was recorded with an analytical balance (Sartorius M-power AZ124) and a Stuart SI500 bioincubator agitating at 100 rpm. After each time step, the

specimens were washed with distilled water and dried in a vacuum oven overnight before weighing, after which they were placed into fresh PBS and lysozyme solution.

Production of nanocomposite microneedle arrays

The microneedle male mould was produced in a "Multijet Modelling" system by Shapeways (U.S.A.) from UV cured acrylic polymer. Female replicated moulds were created by replicating the male mould with silicone (Techsil RTV2420).

Conventional microneedle arrays were created in a two-step process as outlined in figure 1 [11,15], with the filling of the main needle shaft and the filling of the needle base as two separate processes. First, viscous nanocomposite solution (~80 mg ml^{-1}) was used to fill the moulds (figure 1*A–2*). To ensure that the solution filled the full microneedle (tip and shaft), the moulds were centrifuged at 8000 rpm for 1 h. Excess solution was cleaned from the surface and the moulds were left to air dry (figure 1*A–3*). The process of filling, centrifuging and drying the mould was repeated twice more to ensure the shaft was fully formed (figure 1*A–(4–7)*). Secondly, the base was filled with a viscous pristine chitosan solution, centrifuged for 1 h at 8000 rpm and dried in a vacuum oven (figure 1*A–8*). Upon drying, the microneedles were gently removed from the female mould and stored in desiccators.

Detachable microneedle arrays (figure 1*B*) were created with a ring of PEG at the base of the shaft. In an additional step to creating the standard microneedle arrays, after the microneedle shaft has been filled with the nanocomposite mixture and dried, a highly viscous water solution of PEG was applied to the mould and excess solution scraped off (figure 1*B–8*). The moulds were then centrifuged for 1 h at 8000 rpm and dried in a vacuum oven (figure 1*B–9*). The base of the microneedles was created as standard, i.e. filled with high viscosity pristine chitosan solution, centrifuged for 1 h at 8000 rpm and dried in a vacuum oven.

Characterisation of microneedles

A Swift M10L microscope was used for optical microscopy images. Compression testing of the microneedles was carried out with a Hounsfield twin column universal testing machine with a 10 N load cell. The compression rate was 1 mm min^{-1}. Two metal plates were used as the platens; the microneedle array was attached to a fixed platen and a second platen was attached to the load cell and was used to uniformly compress the microneedle arrays (n = 5) [25]. The penetration of the microneedle arrays was measured in full–thickness chicken skin [26] by cross-sectioning the specimen using a Brunel bench microtome after they were embedded in a Labonord Q-Path paraffin embedding medium.

Chitosan–2 wt.% MGQD–LH microneedle arrays (n = 5) were placed in 30 ml of PBS solution (37 ^{o}C, pH = 7.4) and agitated at 100 rpm. LH drug release was measured at set time points by collecting 3 ml of the solution and analysing it with UV-Vis spectroscopy (Perkin Elmer Lambda 900 operating at a resolution of 1nm), having replaced the taken solution with 3 ml of fresh PBS. The curves for each time point were compared to curves of free LH in PBS of known concentrations.

Chitosan–2 wt.% MGQD–BSA microneedle arrays were tested in parallel for both passive diffusion and electrically stimulated diffusion of MGQD–BSA. For passive diffusion, the microneedle array (n = 3) was placed in 100 ml of distilled water (37 ^{o}C). BSA drug release was measured using UV-Vis spectroscopy, similar to the procedure to measure LH release. Electrically stimulated testing of the microneedles was described previously [15]. Briefly, microneedle arrays were mounted to a microscopy slide using double-sided tape and contacts were made with silver paint. The circuit consisted of a prototyping circuit board, a PP3 9 V 280 mAH nickel-metal hydride battery, a 2 kΩ resistor, an on/off switch, and two electrodes. A crocodile clip connected the silver paint contacts to the circuit. The second electrode was submerged in the container of distilled water. The glass slide was submerged

vertically to a point where only the microneedle array was in the water and not the silver paint or the crocodile clip. The electrical flow, therefore, was through the microneedle array and not through the crocodile clip or the silver paint.

Statistical analysis

MatLab 2012a software was used for statistical analysis (t-test, $p < 0.05$) and graphing.

Results and discussion

Characterisation of nanocomposites

Characterisation of the MGQD nanoparticles has been reported before [3], and have been shown to possess photoluminescent and superparamagnetic properties for fluorescent imaging, magnetic resonance imaging (MRI) and responses to external magnetic stimulation. The MGQDs were ~40 nm in diameter and 2–2.5 nm high, and consisted of a GQD core coated with a shell containing a mixture of several iron oxides, namely maghemite, magnetite and hematite.

MGQDs were dispersed within chitosan at concentrations of 0.25–5 wt.%. FT-IR spectra are shown in figure 2A, showing the characteristic peaks of chitosan (N–H peaks at 2800 cm^{-1}, C=O peak at 1720 cm^{-1}, C=C peak at 1640 cm^{-1}, amino peak at 1535–1546 cm^{-1}, C–OH peak at 1405 cm^{-1} and C–O at 1050–1100 cm^{-1}) [27]. The characteristic peaks of MGQDs are shown as C=C at 1564 cm^{-1}, O–C=O at 1406 cm^{-1}, and C–Fe peaks at 1086 cm^{-1} and 1012 cm^{-1} [3,28]. When MGQDs are added to chitosan, the amino peak shifts from 1545 cm^{-1} for pristine chitosan to 1538 cm^{-1} for 1 wt.% MGQD, the C=C peak shifts from 1636 cm^{-1} to 1631 cm^{-1} and the C–O peak shifts from 1060 cm^{-1} to 1063 cm^{-1}. These shifts can be attributed to both the hydrogen bonding that occurs between the chitosan (amino group) [27] and the MGQDs (Fe–O and O–C=O) [3], and for the C–O peak shift there is the possible overlapping of peaks between the C–O peaks of chitosan and the C–Fe peaks of the

MGQDs. The shifts are accompanied by an increase in intensity of the C=C, amino, C–OH and C–O peaks for the 0.25 wt.% to 2 wt.% MGQD nanocomposites.

In figure 2*B*, XRD traces of the nanocomposites can be seen. Typically, the chitosan peaks (crystalline and amorphous) are the only peaks present for both the pristine chitosan and the nanocomposites up to 2 wt.% MGQDs. The diffraction peaks from the MGQDs can be seen in the 5 wt.% nanocomposite due to the relatively high wt.% of MGQDs present. These peaks are the (213) peak from maghemite, (104) from hematite, and (422) and (511) from magnetite [3]. The other MGQD specific peaks may be present but too weak to clearly identify at this wt.%. From the chitosan-specific crystalline peaks that are identified on curve 1 of figure 2*B*, the crystallinity (χ_c) can be determined from Equation 1 [29,30]:

$$\chi_C = \frac{I_C}{I_C + I_A} \quad (1)$$

where I_C and I_A are the peak integrated intensities of the crystalline and amorphous regions, respectively [31,32]. This gives crystallinity values for 0–5 wt.% MGQDs nanocomposites of 34.1%, 27.3%, 27.3%, 27.1%, 26.3% and 25.5% respectively, showing a decrease in crystallinity with increasing wt.% of MGQDs. Graphene based nanoparticles have been shown previously to reduce the crystallinity of some semicrystalline polymers [10,33], presumably due to graphene restricting the polymer chain rearrangement due to the surface absorption and bonding [33].

The electrical conductivity of the nanocomposites was measured, with a maximum conductivity of 3.3 x 10^{-3} S m^{-1} achieved at 5 wt.% MGQD versus 1.5 x 10^{-3} S m^{-1} for pristine chitosan (figure 2*C*). There was no significant increase in conductivity when the MGQDs wt.% increased from 0.25 wt.% to 2 wt.% MGQDs. The conductivity of the 5 wt.% MGQD nanocomposite is lower than that recorded for chitosan–GQD nanocomposites (e.g. 1

wt.% GQD = 1.61 x 10^{-2} S m^{-1}) [15]. The difference between nanocomposites formed of highly-reduced GQD and of MGQD is due to the presence of IO on the surface of the MGQDs. IO can improve the conductivity of polymers [34], but graphene is more conductive than IO [35]. The shape, size, the dispersion degree of the MGQD and the volume fraction of graphene in the nanocomposite are other important factors that affect the electrical conductivity of a nanocomposite [36]. As conductive fillers, MGQDs are not as effective as GQDs, also due to MGQDs being both thicker than GQDs at ~2.5 nm [3] versus ~1.5 nm [15] and of a higher density than the GQDs which means that there is a lower volume fraction of MGQDs within the nanocomposite for a given wt.% (3.66 g cm^{-3} for MGQD in comparison to 1.66 g cm^{-3} for GQD [3]). The 5 wt.% MGQD nanocomposite, although the most conductive with a 94% increase over pristine chitosan and with the highest wt.% of MGQDs for drug delivery, was found to be too brittle to be mechanically tested.

Figure 3*A* shows representative tensile stress-strain curves for pristine chitosan and chitosan nanocomposites. The Young's modulus (E) is 1.48 (± 0.38) GPa, the ultimate tensile strength (UTS) is 62.5 (± 9.4) MPa, and elongation to break (ε_b) is 15.5 (± 4.2) % for pristine chitosan [15]. The 0.5 wt.% and 1 wt.% MGQD nanocomposites can be seen to have a lower UTS than pristine chitosan, with average values of 48.9 (± 3.4) MPa and 49.8 (± 4.1) MPa, respectively. The E of the 0.5 wt.% and 1 wt.% MGQD nanocomposites are 1.19 (± 0.07) GPa and 1.32 (± 0.16) GPa respectively. The 2 wt.% MGQD nanocomposite has a UTS and E that is statistically similar to pristine chitosan, with an E of 1.45 (± 0.27) GPa and a UTS of 60.6 (± 7.3) MPa.

The influential factors are the crystallinity of the chitosan and the effectiveness of the MGQD as reinforcing nanofillers. The crystallinity of a polymer can affect its mechanical properties [37], and the nanocomposites of 0.25–5 wt.% have a lower crystallinity than the pristine chitosan, potentially reducing the strength and stiffness of the nanocomposites. As

discussed previously, MGQD may not be as effective a nanofiller as GO or rGO due to its smaller aspect ratio (it has a smaller diameter than GO or rGO and is thicker than GO at ~2.5 nm [3] versus ~1 nm [10]). It is also denser than rGO (1.46 g cm^{-3} [11]) which means that there is a lower volume fraction of MGQD nanoparticles within the nanocomposite for a given wt.% of nanofiller. MGQD does, however, have a rGO backbone (reported E of 250 GPa [38]) and a shell of IO (E reported as 200–250 GPa depending on the crystal orientation [39]). There is also a relatively strong bonding between the MGQD and the chitosan as discussed before. However, the effectiveness of MGQD being a reinforcing nanofiller is cancelled out by the decrease in crystallinity in the case of the 2 wt.% nanocomposite, and is overshadowed by the latter in the cases of the nanocomposite with lower wt.% MGQD. The ε_b is 13.3 (± 3.9) % for 0.5 wt.%, 15.5 (± 4.5) % for 1 wt.%, and 18.2 (± 4.6) % for 2 wt.% MGQD nanocomposites. The slight increase in ε_b for the 2 wt.% MGQD nanocomposite can be explained by the reduction in the crystallinity of the chitosan in the nanocomposite and that the MGQD may possess a degree of mobility within the nanocomposite when the nanocomposite is under tension, which will absorb energy [40,41].

Pristine chitosan and the 0.5–2 wt.% nanocomposites were subjected to a biodegradation test to determine the effect of MGQD concentration on the biodegradation rate of chitosan. Figure 3*B* shows the effect that increasing the MGQD concentration has upon the remaining mass of chitosan at each time-step when subjected to enzymatic biodegradation. Lysozyme is a natural enzyme and degrades the acetyl units of chitosan through hydrolysis of the β-glycosidic linkages [42,43]. Chitosan samples were reduced to 61.6% of their original mass after 49 days, while 0.5 wt.%, 1 wt.% and 2 wt.% were reduced to 54.1%, 53.8% and 56.2% respectively.

It was previously noted that the inclusion of graphene nanosheets impeded the biodegradation rate of nanocomposites [10,11,44] through the “tortuous path” model [45,46];

this model proposes that high aspect ratio nanosheets that are well dispersed within the polymer matrix would pose a barrier to the permeation of gases or liquids into the matrix [45,46]. This was not the case with the MGQDs with a lower aspect ratio, as the nanocomposites can be seen in figure 3*B* to have a higher biodegradation rate than pristine chitosan and therefore the MGQDs did not impede the enzyme from permeating through the chitosan, similar to our previous work on chitosan–GQD nanocomposites which also contain low–aspect–ratio GQDs [15]. For the chitosan–MGQD nanocomposites, the difference in the final mass of the samples is statistically insignificant, showing that the biodegradation rate is not concentration dependent. The decrease in remaining mass between pristine chitosan and the MGQD nanocomposites is due to the lower crystallinity of the nanocomposites compared to pristine chitosan and the possible diffusion of some of the MGQDs from the nanocomposite into the PBS solution [47,48].

The 2 wt.% MGQD nanocomposite was selected for use as a microneedle array as the nanocomposite had better mechanical properties than the other nanocomposites, while the high wt.% did not hinder the biodegradation characteristics (figure 3*B*) and would allow for a higher quantity of drug to be loaded into the nanocomposite relative to lower wt.% nanocomposites.

Chitosan–2 wt.% microneedle arrays

Chitosan–2 wt.% MGQDs nanocomposites were used to form microneedle arrays for the delivery of small and large MWt drugs into the body via transdermal drug delivery. Previously, it was shown that MGQDs were not cytotoxic to fibroblasts up to a concentration of 50 μg ml^{-1} after 24 h's incubation [3]. Further improvements in cell viability may occur by coating MGQDs by chitosan, similar to the effect that coating GQDs with amine groups and IO by pullulan had [49,50]. Additionally, steam sterilisation/autoclaving has been shown to have minimal effect on chitosan, therefore preserving the chitosan structure within the

microneedle [51]. Figure 4*A* and 4*B* show optical micrographs of the chitosan–2 wt.% MGQD microneedle array (from here on known as CH–MGQD microneedle array), showing the plan and side profile of the microneedle arrays. Their structural integrity under the force of insertion (1.6 N for the microneedle array) [52,53] was verified by compression testing, as seen in figure 4*C*. A failure would be seen as a substantial drop in the compressive force required to compress the microneedle array. The inset of figure 4*C* shows that the CH–MGQD microneedle arrays were strong enough to survive insertion into chicken skin by hand. The depth of penetration of the microneedle array into the chicken skin can be determined as approximately 500 μm, similar to previously reported penetration values for chitosan–GQD microneedles [15].

To allow for the microneedles to detach from the microneedle array base, a disc of the water soluble polymer PEG was included at the base of the microneedle shaft. Different MWt PEG polymers (10k, 20k and 35k) were investigated for their effect on the structural integrity of the microneedle arrays. Higher MWt PEG was not tested as both the systemic clearance of PEG from the body [54] and the dissolution rate [55] are reduced as the MWt increases. Figure 5*A* shows representative curves of the compressive testing of pristine chitosan microneedle arrays with a small ring of PEG between the main microneedle shaft and the base. The 10k PEG microneedle array deformed substantially in comparison to pristine chitosan; the low MWt PEG offered limited mechanical strength to the base of the microneedle when under compression. In contrast, the 20k PEG microneedle arrays retained similar levels of deformation to the pristine chitosan sample due to the stronger 20k PEG relative to the 10k PEG.

The microneedle arrays containing 35k PEG were less ductile than the pristine chitosan microneedle arrays, due again to the rigidity of the high MWt PEG. A strong base is important to prevent the fracture or bending during insertion. The 35k PEG was the strongest

base material and the force versus displacement curve was similar to the chitosan–2 wt.% MGQD microneedle array in figure 4*C*. The 35k PEG was chosen to be used in this nanocomposite microneedle array.

The compressive testing results of the CH–MGQD with 35k PEG (from here on known as CH–MGQD–PEG) microneedle arrays are shown in figure 5*B*, which shows that the addition of a PEG ring to the base of the microneedle main shaft does not deteriorate the strength of the microneedle array in comparison to conventional CH–MGQD microneedle arrays.

Figure 6 shows the detachment of the microneedle main shaft from the array base; the CH–MGQD–PEG microneedle array was mounted to a glass slide and two drops of distilled water were applied to the upper surface. After 5 min, the water had caused the microneedle to swell and upon further inspection the microneedle shafts were no longer connected to the microneedle base. The mounds at the base of the microneedle shaft can be seen to have remained, as seen in figure 6*B* and measuring 310 μm in diameter. The region where PEG was deposited would have been between the mound and the main shaft. This shows that the microneedles can be detached within 5 min when in the presence of water or bodily fluid within skins by placing a ring of PEG between the main shaft and the base. As a further proof of concept test, the CH–MGQD–PEG microneedle array was inserted into chicken skin (figure 6*C*) for 5 min and the microneedles separated from the main base. This further confirms that the PEG separation method can work after insertion into skin.

For the delivery of small MWt therapeutics, LH (MWt = 288) was chosen as the model drug. The drug was bonded (via hydrogen bonding and π-π stacking) to the surface of the MGQDs, with a loading ratio of 0.31:1 (LH:MGQD) [3]. Microneedle arrays containing chitosan and 2 wt.% MGQD with bonded LH were tested for the release of LH (figure 7). Two types of microneedle arrays were tested; CH–MGQD–PEG and CH–MGQD. It can be

seen that the two types of microneedle array were initially (up to 4 h) very similar in terms of quantity of drug released and the rate at which it was released, after which the CH–MGQD–PEG released less LH than the CH–MGQD microneedle array (after 7 h, CH–MGQD released 12.3 µg or 76.6% of the available drug and CH–MGQD–PEG released 9.4 µg or 59.4%). After this time-point, the microneedles were no longer fully intact and the test was stopped.

The difference in final delivery quantity is presumably due to the separation of the microneedles from the base, as the same amount of drug-containing chitosan–2wt.% MGQD was used in both types of microneedles (i.e. three centrifuge cycles) and therefore the results should be identical. It is possible that some of the microneedle shafts for the CH–MGQD–PEG may have become buoyant after 4 h after detaching from the base and floated to the surface of the PBS, but this would not occur during *in vivo* treatment as the microneedles would be embedded in the skin prior to the separation. This test focused on the release of MGQD–LH from the microneedle array; it has been shown that bound, small MWt drugs like LH bound to MGQD [3] or FL bound to rGO [56] can be released from their nanoparticles over a period of time and the nanoparticles can be excreted from the body through urine [57].

To study the release of large MWt drugs from the CH–MGQD microneedles, MGQDs were bonded to the therapeutic BSA (~60k MWt). Iontophoresis could not be achieved with CH–MGQD–PEG microneedles as the PEG ring would cause the detachment of the main microneedle shaft before the drug could be released. Figure 8*A* shows the TGA curves of MGQDs, BSA, and MGQD–BSA. This shows that there is a 9.5%, or 0.10:1 BSA:MGQD, loading of BSA in MGQD–BSA, as determined from the mass loss of MGQD–BSA between 220–400 °C, accounting for both the loss of BSA over this temperature range (52.8%) and absorbed water. This MGQD–BSA was used to form CH–MGQD microneedles which were subsequently tested for passive diffusion release of BSA

over 1440 min (24 h), as shown in figure 8*B*. The release of BSA was limited, with only 0.5 µg or 10.7% released after 9 h and 1.2 µg or 25.7% released over 24 h. Similar passive drug release performance from BSA loaded CH–MGQD–PEG microneedle array is expected.

This low level of release can be improved by using electrical stimulation as shown previously for other therapeutic substances, through either electroporation (where the electrical stimulus increases the permeability of the cell membrane) or iontophoresis (where electrical stimulation creates an electo-repulsion of charged molecules or electro-osmosis of molecules without a charge) [8, 58-60]. The use of electrical stimulation to improve the release of large MWt drugs was shown to be successful for chitosan–GQD microneedles, where there was a significant improvement over standard diffusion release of BSA from chitosan–GQD microneedles [15]. A similar improvement was noted for the CH–MGQD microneedles, with 1.9 µg or 40.7% released over 9 h and 4.5 µg or 96.4% released over 24 h, with the final value markedly higher than the 1.2 µg after 24 h for the passive diffusion microneedle array. Figure 8*C* shows the difference in release visually, with passive diffusion shown in the left container and electrically stimulated release in the right container. The yellow colour of the FL–labelled BSA can be seen in the right container after 4 h, with the colour becoming more vibrant at 6 h and 8 h. After 24 h, the colour of the right container is a combination of the strong yellow from the FL release and the black of the MGQDs [3,15]. The water in the left container does not exhibit a strong yellow colour as the amount of BSA released from the passive diffusion microneedle array was substantially lower. The results of the drug test in figure 8*B* show that chitosan and 2 wt.% MGQD microneedle arrays can be used for the release of large MWt drugs through electrically stimulated diffusion; this ability is due to the nanocomposites being electrical conductive which

enables the current to flow through the nanocomposite in order to transfer the therapeutic from the nanocomposite into the target medium, such as with normal iontophoretic devices and their electrodes [60]. The results presented in figure 7 and figure 8 show that chitosan–MGQD nanocomposites are capable of the efficient and strong release of small and large MWt drugs when in the form of a microneedle array.

Conclusions

Quantum dots of iron oxide coated reduced graphene oxide were dispersed in chitosan to form nanocomposites for transdermal drug delivery applications. The presence of 2 wt.% MGQDs in chitosan increased the electrical conductivity by 25%, which was crucial for the subsequent introduction of electrical simulation during drug delivery. It gave a statistically similar ultimate tensile strength and Young's modulus to chitosan, partially attributable to its lower crystallinity. It also enhanced the biodegradation rate of chitosan slightly during the test period (within 7 weeks).

The nanocomposites were formed into microneedle array by solution casting, and compression testing of the microneedles confirmed that they were strong enough to survive the force of insertion into the skin layers. To allow for the quick detachment of the main microneedle shaft from the array base, the microneedle arrays were manufactured to separate into two parts by the addition of a section of water soluble, biocompatible polymer (PEG) at the base of the microneedles. This allowed for the detachment of the microneedles within 5 min when in contact with water, but did not negatively impact the mechanical strength of the microneedles under compressive loading. The detached microneedle shaft can stay in the body while the base can be readily removed and sent to waste.

Both the conventional and the detachable microneedle array were tested for the release of a small molecular weight drug, with the former releasing 76.6% and the latter releasing 59.4% of the available drug within 7 h. There was a marked improvement in the delivery of large MWt drugs when the conventional microneedles were electrically stimulated to create a microneedle array-iontophoretic type device. The total percentage of drug released increased from 25.7% for passive diffusion to 96.4% over 24 h for the iontophoretic type microneedle array, showing that the ability to efficiently release large MWt drugs from the nanocomposite was achievable by using electrical stimulation of the conductive microneedles.

Microneedles prepared from chitosan–MGQD nanocomposites have great potential for use in medicine; the use of MGQDs as a drug carrier allows for therapeutics of small or large MWt to be bonded to the nanoparticle, subsequently targeted by an external magnetic field to a site of release whilst being monitored by MRI or fluorescent imaging. The electrical conductivity of chitosan–MGQD nanocomposites can be used for the electrically stimulated release of large MWt drugs, enabling chitosan–MGQD microneedle arrays to be used as a universal delivery platform for therapeutics of different sizes and their subsequent targeting and tracking.

Data Accessibility

The data are available as the electronic supplementary material.

Authors' Contributions

B.C. conceived the project. R.J. performed the experiments. R.J. and B.C. designed the experiments, analysed the data and wrote the paper.

Funding

The authors thank the British Council and the Department of Business, Innovation and Skills for a Global Innovation Initiative grant (GII207).

References

1. Marcano DC, Kosynkin D V, Berlin JM, Sinitskii A, Sun Z, Slesarev A, Alemany LB, Lu W, Tour JM. 2010 Improved synthesis of graphene oxide. *ACS Nano* **4**, 4806–4814. (doi:10.1021/nn1006368)

2. Bao H, Pan Y, Ping Y, Sahoo NG, Wu T, Li L, Li J, Gan LH. 2011 Chitosan-functionalized graphene oxide as a nanocarrier for drug and gene delivery. *Small* **7**, 1569–1578. (doi:10.1002/smll.201100191)

3. Justin R *et al.* 2016 Photoluminescent and superparamagnetic reduced graphene oxide–iron oxide quantum dots for dual-modality imaging, drug delivery and photothermal therapy. *Carbon* **97**, 54–70. (doi:10.1016/j.carbon.2015.06.070)

4. Jung JH, Cheon DS, Liu F, Lee KB, Seo TS. 2010 A graphene oxide based immuno-biosensor for pathogen detection. *Angew. Chem. Int. Ed. Engl.* **49**, 5708–11. (doi:10.1002/anie.201001428)

5. Liu Y, Yu D, Zeng C, Miao Z, Dai L. 2010 Biocompatible graphene oxide-based glucose biosensors. *Langmuir* **26**, 6158–60. (doi:10.1021/la100886x)

6. Robinson JT, Tabakman SM, Liang Y, Wang H, Casalongue HS, Vinh D, Dai H. 2011 Ultrasmall reduced graphene oxide with high near-infrared absorbance for photothermal therapy. *J. Am. Chem. Soc.* **133**, 6825–6831. (doi:10.1021/ja2010175)

7. Sun X, Liu Z, Welsher K, Robinson JT, Goodwin A, Zaric S, Dai H. 2008 Nano-Graphene Oxide for Cellular Imaging and Drug Delivery. *Nano Res.* **1**, 203–212. (doi:10.1007/s12274-008-8021-8)

8. Weaver CL, LaRosa JM, Luo X, Cui XT. 2014 Electrically controlled drug delivery from graphene oxide nanocomposite films. *ACS Nano* **8**, 1834–1843. (doi:10.1021/nn406223e)

9. Piao Y, Chen B. 2015 Self-assembled graphene oxide-gelatin nanocomposite hydrogels: Characterization, formation mechanisms, and pH-sensitive drug release behavior. *J. Polym. Sci. Part B Polym. Phys.* **53**, 356–367. (doi:10.1002/polb.23636)

10. Justin R, Chen B. 2014 Characterisation and drug release performance of biodegradable chitosan–graphene oxide nanocomposites. *Carbohydr. Polym.* **103**, 70–80. (doi:10.1016/j.carbpol.2013.12.012)

11. Justin R, Chen B. 2014 Strong and conductive chitosan-reduced graphene oxide nanocomposites for transdermal drug delivery. *J. Mater. Chem. B* **2**, 3759–3770. (doi:10.1039/c4tb00390j)

12. Yong K-T. 2009 Mn-doped near-infrared quantum dots as multimodal targeted probes for pancreatic cancer imaging. *Nanotechnology* **20**, 15102–15112. (doi:10.1088/0957-4484/20/1/015102)

13. Archer PI, Santangelo SA, Gamelin DR. 2007 Direct Observation of sp-d exchange interactions in colloidal Mn2+- and Co2+-doped CdSe quantum dots. *Nano Lett.* **7**, 1037–1043. (doi:10.1021/nl0702362)

14. Kim J *et al.* 2006 Magnetic fluorescent delivery vehicle using uniform mesoporous silica spheres embedded with monodisperse magnetic and semiconductor nanocrystals. *J. Am. Chem. Soc.* **128**, 688–689. (doi:10.1021/ja0565875)

15. Justin R, Roman S, Chen D, Tao K, Geng X, Grant RT, MacNeil S, Sun K, Chen B. 2015 Biodegradable and conductive chitosan–graphene quantum dot nanocomposite microneedles for delivery of both small and large molecular weight therapeutics. *RSC Adv.* **5**, 51934–51946. (doi:10.1039/C5RA04340A)

16. Kumar MNVR, Muzzarelli RAA, Muzzarelli C, Sashiwa H, Domb AJ. 2004 Chitosan chemistry and pharmaceutical perspectives. *Chem. Rev.* **104**, 6017–6084. (doi:10.1021/cr030441b)

17. Arora A, Prausnitz MR, Mitragotri S. 2008 Micro-scale devices for transdermal drug delivery. *Int. J. Pharm.* **364**, 227–236. (doi:10.1016/j.ijpharm.2008.08.032)

18. Widera G, Johnson J, Kim L, Libiran L, Nyam K, Daddona PE, Cormier M. 2006 Effect of delivery parameters on immunization to ovalbumin following intracutaneous administration by a coated microneedle array patch system. *Vaccine* **24**, 1653–1664. (doi:10.1016/j.vaccine.2005.09.049)

19. Koutsonanos DG, del Pilar Martin M, Zarnitsyn VG, Sullivan SP, Compans RW, Prausnitz MR, Skountzou I. 2009 Transdermal influenza immunization with vaccine-coated microneedle arrays. *PLoS One* **4**, 4773–4782. (doi:10.1371/journal.pone.0004773)

20. Cormier M, Johnson B, Ameri M, Nyam K, Libiran L, Zhang DD, Daddona P. 2004 Transdermal delivery of desmopressin using a coated microneedle array patch system. *J. Control. Release* **97**, 503–511. (doi:10.1016/j.jconrel.2004.04.003)

21. Davis SP, Martanto W, Allen MG, Prausnitz MR. 2005 Hollow metal microneedles for insulin delivery to diabetic rats. *IEEE Trans. Biomed. Eng.* **52**, 909–915. (doi:10.1109/TBME.2005.845240)

22. Gupta J, Gill HS, Andrews SN, Prausnitz MR. 2011 Kinetics of skin resealing after insertion of microneedles in human subjects. *J. Control. Release* **154**, 148–155. (doi:10.1016/j.jconrel.2011.05.021)

23. Chu LY, Prausnitz MR. 2011 Separable arrowhead microneedles. *J. Control. Release* **149**, 242–249. (doi:10.1016/j.jconrel.2010.10.033)

24. Brouwer J, van Leeuwen-Herberts T, de Ruit MO. 1984 Determination of lysozyme in serum, urine, cerebrospinal fluid and feces by enzyme immunoassay. *Clin. Chim. Acta* **142**, 21–30. (doi:10.1016/0009-8981(84)90097-4)

25. Tsioris K, Raja WK, Pritchard EM, Panilaitis B, Kaplan DL, Omenetto FG. 2012 Fabrication of Silk Microneedles for Controlled-Release Drug Delivery. *Adv. Funct. Mater.* **22**, 330–335. (doi:10.1002/adfm.201102012)

26. Sammoura F, Kang J, Heo Y-M, Jung T, Lin L. 2007 Polymeric microneedle fabrication using a microinjection molding technique. *Microsyst. Technol.* **13**, 517–522. (doi:10.1007/s00542-006-0204-1)

27. Han D, Yan L, Chen W, Li W. 2011 Preparation of chitosan/graphene oxide composite film with enhanced mechanical strength in the wet state. *Carbohydr. Polym.* **83**, 653–658. (doi:10.1016/j.carbpol.2010.08.038)

28. Ramalakshmi M, Shakkthivel P, Sundrarajan M, Chen SM. 2013 Novel method of room temperature ionic liquid assisted Fe3O4 nanocubes and nanoflakes synthesis. *Mater. Res. Bull.* **48**, 2758–2765. (doi:10.1016/j.materresbull.2013.03.024)

29. Nunes C, Mahendrasingam A, Suryanarayanan R. 2005 Quantification of crystallinity in substantially amorphous materials by synchrotron X-ray powder diffractometry. *Pharm. Res.* **22**, 1942–1953. (doi:10.1007/s11095-005-7626-9)

30. Galvan-Sanchez A, Urena-Nunez F, Flores-Llamas H, Lopez-Castanares R. 1999 Determination of the crystallinity index of iron polymethacrylate. *J. Appl. Polym. Sci.* **74**, 995–1002. (doi:10.1002/(SICI)1097-4628(19991024)74:4<995::AID-APP26>3.0.CO;2-N)

31. Pan Y, Wu T, Bao H, Li L. 2011 Green fabrication of chitosan films reinforced with parallel aligned graphene oxide. *Carbohydr. Polym.* **83**, 1908–1915. (doi:10.1016/j.carbpol.2010.10.054)

32. Yang X, Tu Y, Li L, Shang S, Tao X-M. 2010 Well-dispersed chitosan/graphene oxide nanocomposites. *ACS Appl. Mater. Interf.* **2**, 1707–1713. (doi:10.1021/am100222m)

33. Chaudhry AU, Mittal V. 2013 High-density polyethylene nanocomposites using masterbatches of chlorinated polyethylene/graphene oxide. *Polym. Eng. Sci.* **53**, 78–88. (doi:10.1002/pen.23241)

34. Sun DC, Sun DS. 2009 The synthesis and characterization of electrical and magnetic nanocomposite: PEDOT/PSS–Fe3O4. *Mater. Chem. Phys.* **118**, 288–292. (doi:10.1016/j.matchemphys.2009.07.060)

35. Stoller MD, Park S, Zhu Y, An J, Ruoff RS. 2008 Graphene-based ultracapacitors. *Nano Lett.* **8**, 3498–3502. (doi:10.1021/nl802558y)

36. Potts JR, Dreyer DR, Bielawski CW, Ruoff RS. 2011 Graphene-based polymer nanocomposites. *Polymer (Guildf).* **52**, 5–25. (doi:10.1016/j.polymer.2010.11.042)

37. Halpin JC. 1972 Moduli of Crystalline Polymers Employing Composite Theory. *J. Appl. Phys.* **43**, 2235–2241. (doi:10.1063/1.1661482)

38. Gómez-Navarro C, Burghard M, Kern K. 2008 Elastic properties of chemically derived single graphene sheets. *Nano Lett.* **8**, 2045–2049. (doi:10.1021/nl801384y)

39. Kester E, Rabe U, Presmanes L, Tailhades P, Arnold W. 2000 Measurement of Young's modulus of nanocrystalline ferrites with spinel structures by atomic force acoustic microscopy. *J. Phys. Chem. Solids* **61**, 1275–1284. (doi:10.1016/S0022-3697(99)00412-6)

40. Dasari A, Yu Z-Z, Mai Y-W. 2007 Transcrystalline Regions in the Vicinity of Nanofillers in Polyamide-6. *Macromolecules* **1**, 123–130. (doi:10.1021/ma0621122)

41. Wan C, Chen B. 2012 Reinforcement and interphase of polymer/graphene oxide nanocomposites. *J. Mater. Chem.* **22**, 3637–3646. (doi:10.1039/c2jm15062j)

42. Freier T, Koh HS, Kazazian K, Shoichet MS. 2005 Controlling cell adhesion and degradation of chitosan films by N-acetylation. *Biomaterials* **26**, 5872–5878. (doi:10.1016/j.biomaterials.2005.02.033)

43. Nordtveit RJ, Vårum KM, Smidsrød O. 1994 Degradation of fully water-soluble, partially N-acetylated chitosans with lysozyme. *Carbohydr. Polym.* **23**, 253–260. (doi:10.1016/0144-8617(94)90187-2)

44. Depan D, Shah JS, Misra RDK. 2013 Degradation mechanism and increased stability of chitosan-based hybrid scaffolds cross-linked with nanostructured carbon: Process–structure–functional property relationship. *Polym. Degrad. Stab.* **98**, 2331–2339. (doi:10.1016/j.polymdegradstab.2013.08.007)

45. Nielsen LE. 1967 Models for the Permeability of Filled Polymer Systems. *J Macromol Sci, Part A. Pure Appl Chem* **1**, 929–942. (doi:10.1080/10601326708053745)

46. Sun L, Boo W-J, Clearfield A, Sue H-J, Pham HQ. 2008 Barrier properties of model epoxy nanocomposites. *J. Membr. Sci.* **318**, 129–136. (doi:10.1016/j.memsci.2008.02.041)

47. Francis Suh J-K, Matthew HW. 2000 Application of chitosan-based polysaccharide biomaterials in cartilage tissue engineering: a review. *Biomaterials* **21**, 2589–2598. (doi:10.1016/S0142-9612(00)00126-5)

48. Depan D, Pratheep Kumar A, Singh RP, Misra RDK. 2014 Stability of chitosan/montmorillonite nanohybrid towards enzymatic degradation on grafting with poly(lactic acid). *Mater. Sci. Technol.* **30**, 587–592. (doi:10.1179/1743284713Y.0000000501)

49. Jiang F *et al.* 2013 Eco-friendly synthesis of size-controllable amine-functionalized graphene quantum dots with antimycoplasma properties. *Nanoscale* **5**, 1137–1142. (doi:10.1039/c2nr33191h)

50. Gupta AK, Gupta M. 2005 Cytotoxicity suppression and cellular uptake enhancement of surface modified magnetic nanoparticles. *Biomaterials* **26**, 1565–1573. (doi:10.1016/j.biomaterials.2004.05.022)

51. Juan AS, Montembault A, Gillet D, Say JP, Rouif S, Bouet T, Royaud I, David L. 2012 Degradation of chitosan-based materials after different sterilization treatments. *IOP Conf. Ser. Mater. Sci. Eng.* **31**, 12007–12012. (doi:10.1088/1757-899X/31/1/012007)

52. Henry S, McAllister D, Allen M, Prausnitz M. 1998 Microfabricated microneedles: A novel approach to transdermal drug delivery. *J. Pharmacol. Sci.* **87**, 922–925. (doi:10.1021/js980042+)

53. Aggarwal P. 2004 Geometrical effects in mechanical characterizing of microneedle for biomedical applications. *Sensors Actuators B Chem.* **102**, 226–234. (doi:10.1016/j.snb.2004.04.024)

54. M J Knauf, Bell DP, Hirtzer P, Luo ZP, Young JD, Katre N V. 1988 Relationship of effective molecular size to systemic clearance in rats of recombinant interleukin-2 chemically modified with water-soluble polymers. *J. Biol. Chem.*, 15064–15070. (doi:N/A)

55. Okonogi S, Puttipipatkhachorn S. 2006 Dissolution improvement of high drug-loaded solid dispersion. *AAPS PharmSciTech* **7**, E52. (doi:10.1208/pt070252)

56. Justin R, Chen B. 2014 Body temperature reduction of graphene oxide through chitosan functionalisation and its application in drug delivery. *Mater. Sci. Eng. C.* **34**, 50–53. (doi:10.1016/j.msec.2013.10.010)

57. Huang X *et al.* 2013 Effect of injection routes on the biodistribution, clearance, and tumor uptake of carbon dots. *ACS Nano* **7**, 5684–5693. (doi:10.1021/nn401911k)

58. Chen H *et al.* 2009 Iontophoresis-driven penetration of nanovesicles through microneedle-induced skin microchannels for enhancing transdermal delivery of insulin. *J. Control. Release* **139**, 63–72. (doi:10.1016/j.jconrel.2009.05.031)

59. Denet A.-R., Vanbever R., Preat V. 2004 Skin electroporation for transdermal and topical delivery. *Adv. Drug Deliv. Rev.* **56**, 659–674. (doi:10.1016/j.addr.2003.10.027)

60. Brown MB, Traynor MJ, Martin GP, Akomeah FK. 2008 Transdermal drug delivery systems: skin perturbation devices. *Methods Mol. Biol.* **437**, 119–139. (doi:10.1007/978-1-59745-210-6_5)

Figure Captions

Figure 1. Experimental procedure to create (A) conventional and (B) detachable chitosan–MGQD microneedle arrays.

Figure 2. (A) FT–IR spectra, (B) XRD traces and (C) electrical conductivity of chitosan–MGQD nanocomposites.

Figure 3. (A) Representative tensile testing curves and (B) biodegradation data for pristine chitosan and 0.5 wt.%, 1 wt.%, and 2 wt.% MGQD nanocomposites.

Figure 4. Optical micrographs of the CH–MGQD microneedle array: (A) side view and (B) plan view, and (C) compression testing curves of CH–MGQD microneedle arrays. (Inset) side view of CH–MGQD microneedle array after insertion into chicken skin showing the penetration depth.

Figure 5. Compression testing of (A) chitosan and various MWt PEGs and (B) CH–MGQDs with 35k PEG microneedle arrays.

Figure 6. Side view of a CH–MGQD–PEG microneedle array, (A) before and (B) after 5 min in the presence of water, showing the successful detachment of the microneedle shaft from the base. (C) After insertion of the microneedle array into chicken skin for 5 min, the successful detachment of the microneedle shaft from the base can be seen again.

Figure 7. Release of LH from microneedle arrays of CH–MGQD or CH–MGQD–PEG over 7 h. The release from both microneedles can be seen to be very similar in profile.

Figure 8. (A) TGA curves showing the loading of BSA onto MGQDs, (B) the passive diffusion and electrically stimulated release of BSA from microneedle arrays, and (C) visual representation of the difference in release of BSA by either passive (left) or electrically stimulated (right) release.

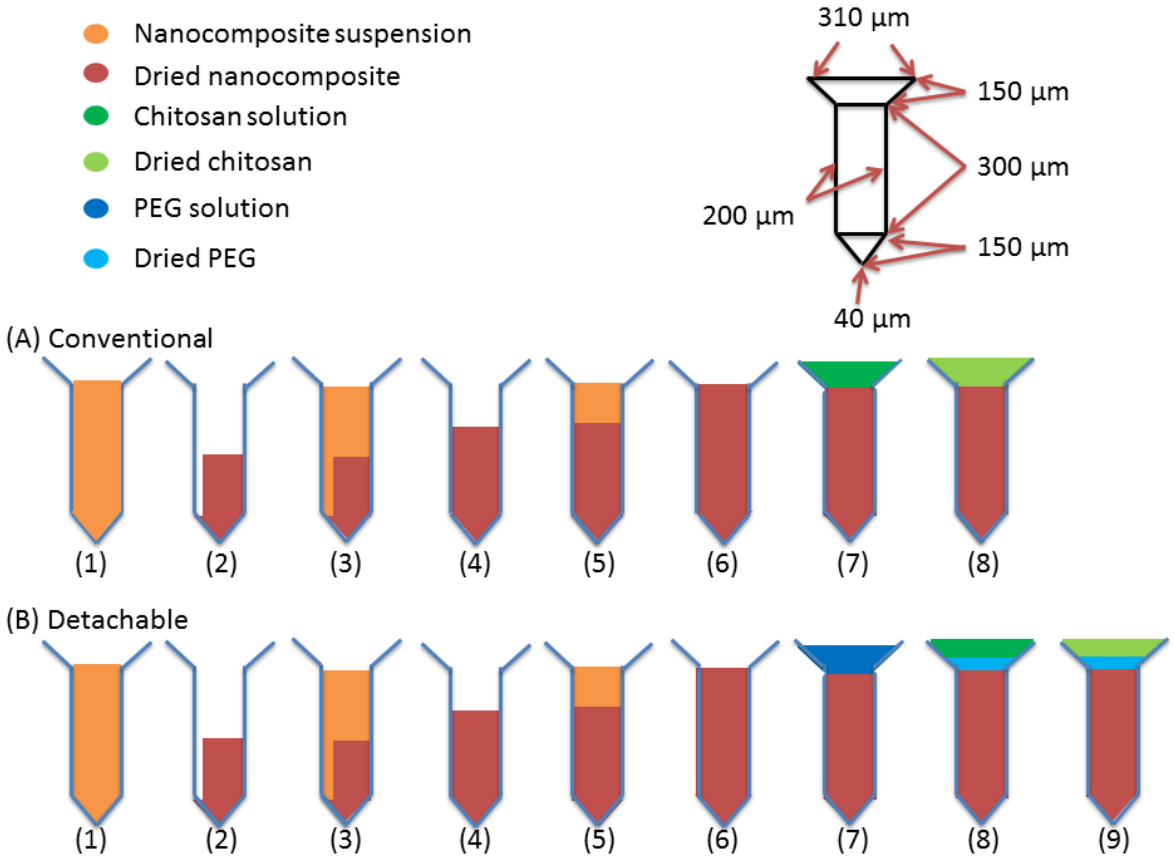
Nanocomposite suspension
Dried nanocomposite
Chitosan solution
Dried chitosan
PEG solution
Dried PEG
310 µm
150 µm
300 µm
200 µm
150 µm
40 µm
(A) Conventional
(1)
(2)
(3)
(4)
(5)
(6)
(7)
(8)
(B) Detachable
(1)
(2)
(3)
(4)
(5)
(6)
(7)
(8)
(9)

Figure 1

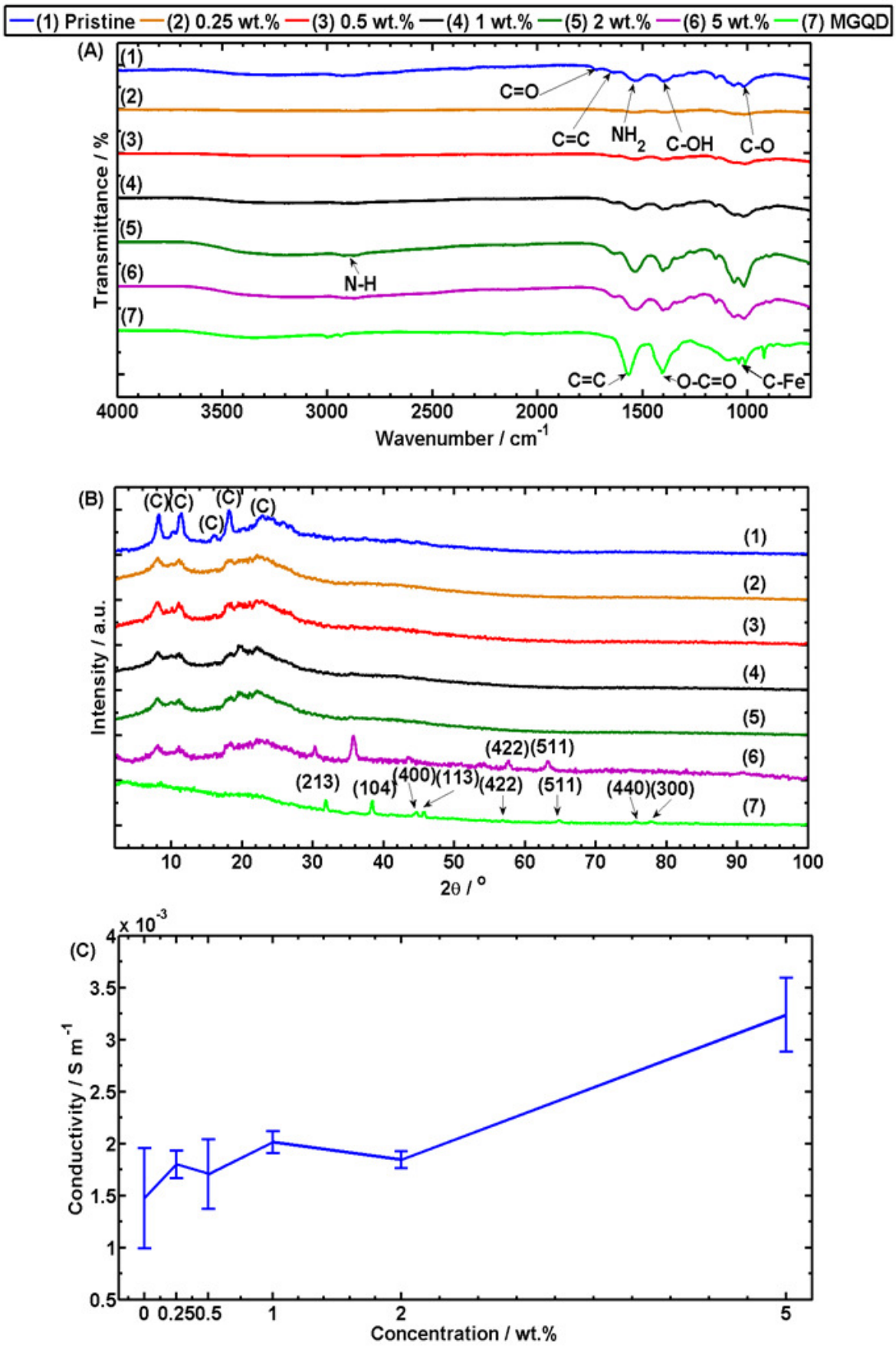
(1) Pristine
(2) 0.25 wt.%
(3) 0.5 wt.%
(4) 1 wt.%
(5) 2 wt.%
(6) 5 wt.%
(7) MGQD
(A)
Transmittance / %
C=O
C=C
NH2
C-OH
C-O
N-H
C=C
O-C=O
C-Fe
Wavenumber / cm-1
(B)
Intensity / a.u.
(213)
(104)
(400)(113)
(422)
(511)
(422)(511)
(440)(300)
2θ / °
(C)
x 10-3
Conductivity / S m-1
Concentration / wt.%

Figure 2

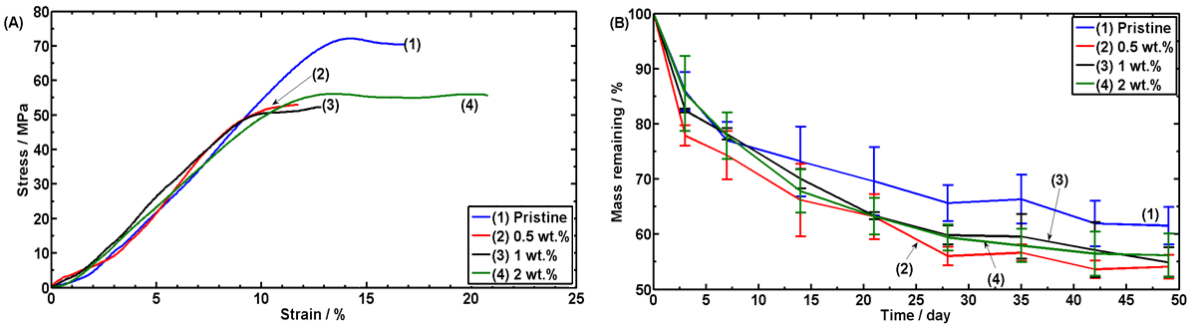

Figure 3

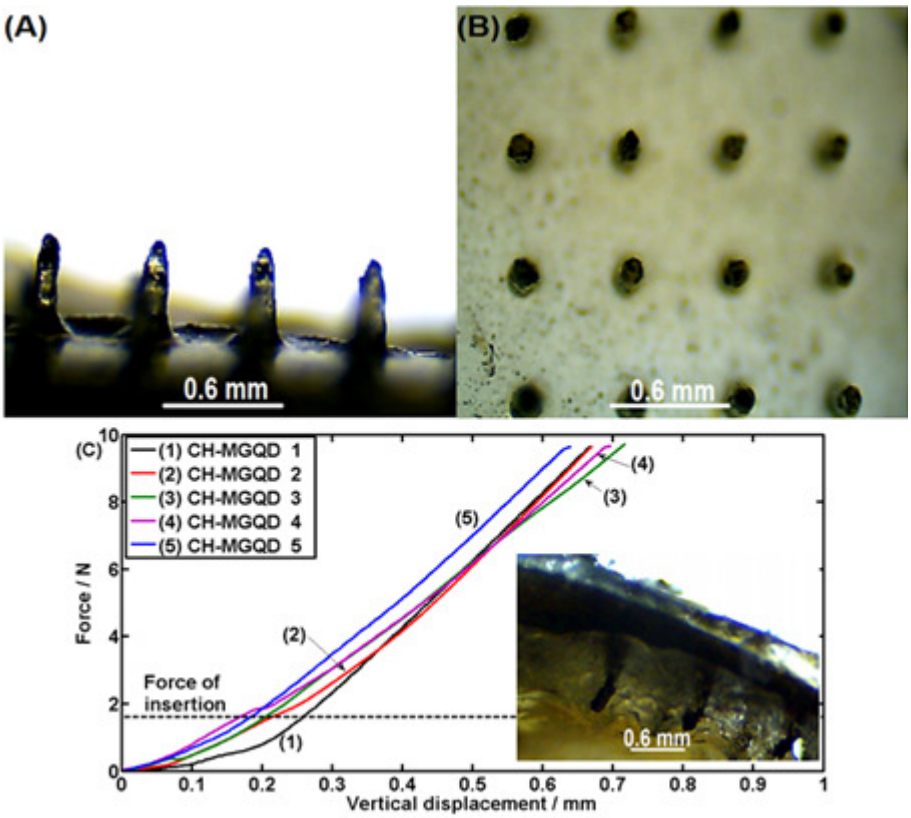

Figure 4

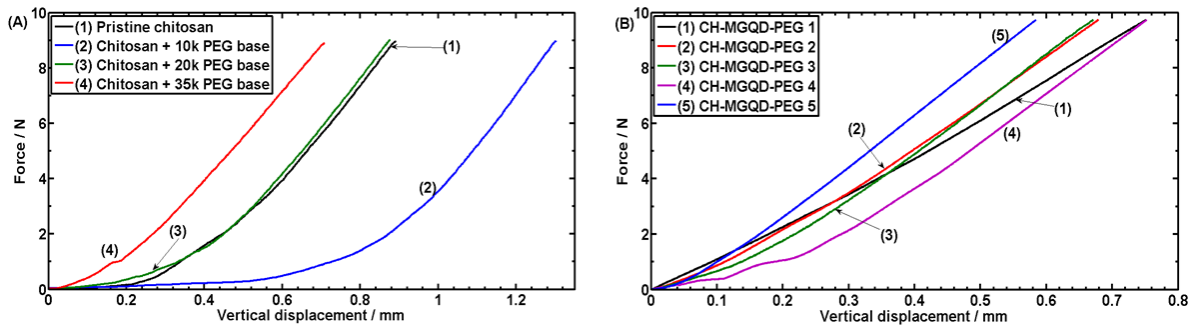

Figure 5

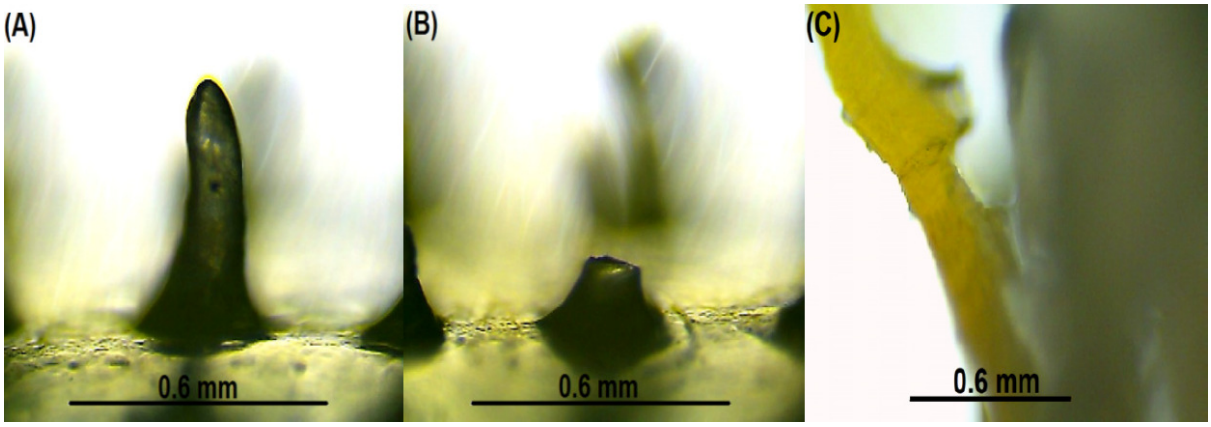

Figure 6

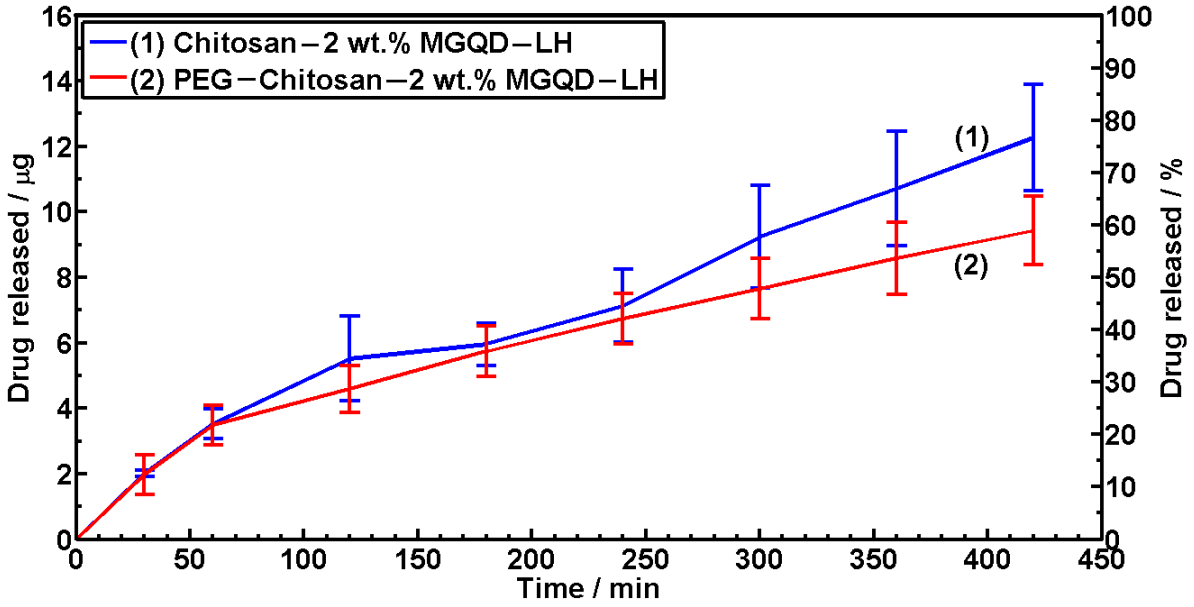

Figure 7

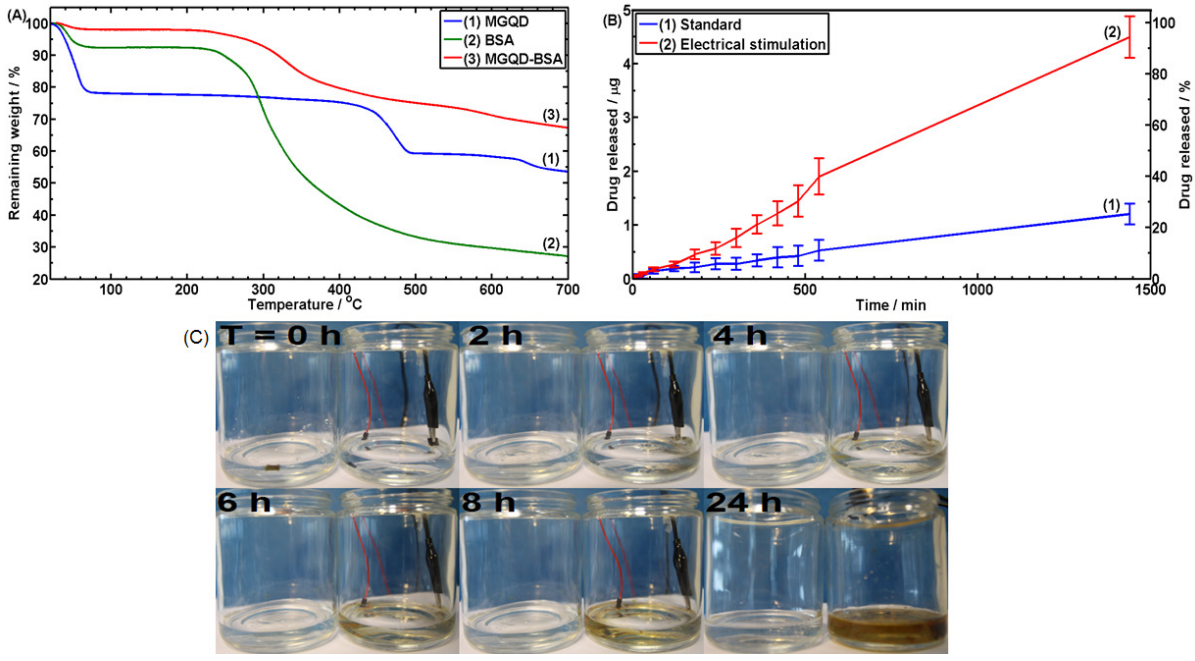

Figure 8